CHEMISTRY
A EUROPEAN JOURNAL

DOI: 10.1002/chem.200700106

On the Coherent Description of Diffusion-Influenced Fluorescence Quenching Experiments

Arnulf Rosspeintner,*[a] Daniel R. Kattnig,[a] Gonzalo Angulo,[a, c] Stephan Landgraf,[a] Günter Grampp,[a] and Alejandro Cuetos[b]

Abstract: The fluorescence quenching by electron transfer of a fluorophore, 2,5-bis(dimethylamino)-1,3-benzenedicarbonitrile, to 1,3-dimethyl-2-nitrobenzene, has been studied by means of time-resolved and steady-state experiments at different viscosities and up to large quencher concentrations. Differential Encounter Theory (DET) has been used to rationalize the results, in combination with electron transfer modelled by the Marcus theory. Additionally, the solvent structure and the hydrodynamic effect on the diffusion coefficient have been taken into account. Any simpler model failed to simultaneously fit all the results. The large number of quencher concentrations used is crucial to unambiguously extract the electron transfer parameters.

Keywords: diffusion · electron transfer · fluorescence · viscosity

Introduction

Fluorescence quenching in solution has been the subject of many works in the past. Bimolecular reactions between the excited fluorophore and a quencher have been studied mainly either by steady-state or time-resolved fluorescence spectroscopies.[1–5] Increasingly, a big number of applications (chemical sensing, biomolecular recognition) base their analysis on the conclusions previously obtained with chemical model systems.[6] These methods have been extensively used to obtain relevant parameters of elementary reactions such as electron, energy or proton transfer. Quenching itself has also been a matter of basic research in statistical mechanics leading to many competing theories, which only recently have been compared critically.[7] Unfortunately, very often the number of experimental data are too low to allow for a clear-cut distinction between these theories.

One of the most intriguing facts, very often observed, is the non-linearity of the Stern–Volmer (SV) plots. A SV plot is constructed from the fluorescence intensity, I, recorded at different quencher concentrations ($I(c=0)/I(c)$ vs c), with a slope equal to the SV constant (K_{SV}), which is defined as the product of the quenching rate constant, κ, and the lifetime of the fluorophore, τ.[1–5] If this quenching rate constant does not depend on the concentration the plot is a straight line. Several reasons can be invoked if a positive deviation is observed at high quencher concentrations: i) ground state complex formation (we refer to this as pseudo-static quenching); ii) excited state quenching without diffusion (static quenching); or iii) diffusion assisted quenching with a non-stationary stage (dynamic quenching).[6] It is very simple to distinguish the first from the other two cases: a change in the absorption or in the fluorescence spectra shapes by adding the quencher and monoexponential fluorescence decays, even at quencher concentrations that show a positive deviation in the SV plots indicate that the reaction occurs in the fluorophore electronic ground state. For charged reactants the positive deviations naturally depend on the ionic strength.[8] We will restrict ourselves to the case of uncharged reactants and no ground state complex formation.

Starting from the simplest to the most complex model of the diffusion assisted reaction, we can describe the fluorescence quenching and the SV plot as follows: If the reaction is not time dependent and there is nothing but contact reac-

[a] Prof. Dr. Dipl.-Ing. A. Rosspeintner, Dipl.-Ing. D. R. Kattnig, Dr. G. Angulo, Prof. Dr. S. Landgraf, Prof. Dr. G. Grampp
Graz University of Technology
Technikerstrasse 4/I, 8010 Graz (Austria)
Fax: (+43) 316-873-8225
E-mail: rosspeintner@tugraz.at

[b] Dr. A. Cuetos
Utrecht University, Princetonplein 5
3584 CC Utrecht (The Netherlands)

[c] Dr. G. Angulo
Present address:
Physical Chemistry Department Sciences II, University of Geneva
Quai Ernest Ansermet 30, 1211 Geneva 4 (Switzerland)

tion, no positive deviation can be observed in the SV plot. This is the case when the reaction is much slower than diffusion (kinetically controlled reaction). Very often when a positive deviation is experimentally observed, the static quenching is treated as a separate and instantaneous step, by means of the sphere of action model.[9] In quite an artificial way, and theoretically difficult to justify, this model has been combined with the subsequent time independent quenching model. Again, a low number of experimental points, or a lack of comparison with the time-resolved experiments, has allowed for an apparently good correlation between these models and the theory.[10–13] In the opposite case, a purely diffusion controlled reaction leads to a time dependent rate constant (this is the first example of a non-Markovian theory in chemical kinetics) as obtained by Smoluchowski in the case of an infinitely fast contact reaction.[14] In this case the SV deviation is present but does not depend on the intrinsic reaction parameters. If the contact reaction is characterized by a given finite rate the Collins–Kimball model can be introduced.[15] In this case, information about the intrinsic reaction rate constant can be obtained from the non-linearity of the SV plot. This model has been used many times in order to obtain electron transfer rate constants, which were then compared with Marcus theory's prediction.[16–21] Very often a small number of points in the curved region of the SV plot and not congruently fitted time-resolved data have led to misleading interpretations. The introduction of the fact that the reaction may take place at distances larger than contact complicates the model.[4] Now, the SV curvature is strongly influenced by the parameters that define the space distribution of the intrinsic rate constant. Several rate models have been applied, such as exponential or step-wise rates, as well as the physically better grounded Marcus model for electron transfer.[4] In such a case a large number of data points is necessary to obtain a unique set of fitting parameters. Congruence between steady-state and time-resolved data is compulsory and gives additional strength to the obtained parameters. In all these increasingly complicated models the solvent is treated as a continuum. Its structure, as described by the solvent–solvent density distribution function (measurable by means of neutron scattering), introduces an attractive potential between the reacting partners at short distances. Finally, the hydrodynamic effect can also be taken into consideration. Basically, it consists of a reduction of the diffusion coefficient at short distances. When the reacting particles approach each other one reaction partner feels how the other one pushes the solvent molecules into its own propagation direction, and vice versa, thus hindering the mutual approach. These two effects are time independent and were both shown to affect diffusion controlled quenching kinetics.[22]

In this article we intend to fill the gap between theory and experiment, and give some hints on how to treat the experimentally extracted data in order to obtain meaningful parameters for the studied elementary reaction. We have chosen an electron transfer reaction for two reasons: Firstly there exists a consistent and well accepted theory describing this process. Secondly, because it may occur off-contact. In the last years, the theory to treat diffusion influenced electron transfer has been well established and supported by all kinds of experiments,[23] but not yet to such a complete quenching data set as this present work, comprising 150 quenching experiments at different viscosities. We are showing how to handle the experimental data in order to obtain a fully consistent description of both time-resolved and steady-state data at different viscosities. Starting from very low to relatively high quencher concentrations the positive deviation in the SV plot increases. A big number of points has been obtained in order to be able to distinguish between various models and decide whether or not solvent structure and hydrodynamic effect have to be taken into account. Additionally, the obtained parameters are used to explain the time-resolved results in a coherent manner. It is clear that both the data point density and the joint analysis of both kinds of data are absolutely necessary to extract a good reaction description.

The article is organized as follows: The theoretical model used and the numerical methods employed for the fitting procedure, are described, as well as the modelling of the solvent for the calculation of the solvent structure, $g(r)$. In the Section "Results and Discussion" the ability to describe the experimental results of all the theoretical models contemplated will be compared. A detailed description of the different approaches to jointly fit to the time-resolved and steady-state results is given because of its relevance to the final interpretation of the results. Finally, an extensive experimental section describes not only the sample preparation and the apparatuses handling, but also the data pretreatment.

Theoretical and Numerical Procedures

Differential Encounter Theory (DET): The diffusion influenced deactivation of excited fluorophores by remote electron transfer is well described by differential encounter theory (DET) provided that all elementary steps are irreversible.[4,23] For the system under investigation the back electron transfer to the excited state is thermodynamically unfavoured and can thus safely be neglected facilitating an analysis in the framework of DET. The central result of DET, as developed in reference [24] and reviewed in [4,23], is that the excited state population, $N(t,c)$, is given by Equation (1):

$$N(t,c) = N_0 \exp\left(-\frac{t}{\tau} - c\int_0^t k(t')\mathrm{d}t'\right) = N_0 R(t) \quad (1)$$

where the time dependent quenching rate, $k(t)$, is related to the pair correlation function, $n(r,t)$, by

$$k(t) = 4\pi \int_\sigma^\infty w(r)n(r,t)r^2\mathrm{d}r \quad (2)$$

Here, $w(r)$ is the distance dependent intrinsic rate of the electron transfer (see below), τ is the fluorescence lifetime of the excited donor, c denotes the acceptor concentration and σ the donor–acceptor contact distance.

The auxiliary function $n(r,t)$ is directly related to the probability density, $n(r,t)/V$, of finding the quencher at a distance r from the excited donor at time t after excitation. Its equation of motion comprises a term accounting for the mutual diffusion, $\hat{\mathcal{L}}(r)n(r,t)$, and a sink term accounting for the deactivation process, $w(r)n(r,t)$:

$$\dot{n}(r,t) = \hat{\mathcal{L}}(r)n(r,t) - w(r)n(r,t) \tag{3}$$

In this study the diffusion operator, $\hat{\mathcal{L}}(r)$, includes an explicit distance dependence of the diffusion coefficient, $D(r)$, and a potential, $u(r)$, associated with the solvent structure, $u(r)=v(r)kT=-kT\ln(g(r))$:

$$\hat{\mathcal{L}}(r) = \frac{1}{r^2}\frac{\partial}{\partial r}r^2 D(r)g(r)\frac{\partial}{\partial r}\frac{1}{g(r)} \tag{4}$$

The r dependence of the diffusion coefficient is due to the hydrodynamic effect, which originates from the inhibition of the solvent molecules to vacate the intervening space when donor and acceptor molecules approach each other.[25] Hence for small interparticle distances, in particular those relevant to the electron transfer process, the diffusion coefficient is decreased substantially. For solvent and solute molecules of similar size an empirical model, proposed by Northrup and Hynes (see also Figure 2),[26] is believed to give the most realistic description of this effect:

$$D_{\mathrm{NH}}(r) = D\left(1-\frac{1}{2}\exp\left(-\frac{r-\sigma}{\sigma}\right)\right) \tag{5}$$

with D denoting the bulk diffusion coefficient. Unlike the model of Deutch and Felderhof, which is based on continuum hydrodynamics, it is an approximation for solvent and solute molecules of similar size.[27] The former model gives the "classical" hydrodynamic result:

$$D_{\mathrm{DF}}(r) = D\left(1-\frac{3\sigma}{4r}\right) \tag{6}$$

for two solutes of same size ($\sigma/2$), being bigger than the solvent molecules.

The donor–acceptor pair distribution function $g(r)$ accounts for the microscopic structure of the condensed phase. For relatively dilute acceptors, that is, in the absence of acceptor–acceptor excluded volume effects, the local density of acceptors about the donor parallels the solvent density variations.[22] Besides giving rise to the appearance of a potential of mean force in Equation (4), the solvent structure changes the initial distribution of acceptors. In fact, sites close to contact about any photoexcited donor are significantly more likely to be occupied by an acceptor than would be expected if the solvent were approximated by a continuum. Thus, the appropriate initial condition to Equation (3) is $n(r,0)=g(r)$.[22] Furthermore, the flux across the boundary at σ has to vanish and, hence, the inner boundary condition reads:

$$4\pi\sigma^2 D(\sigma)\left(\frac{\partial n(r,t)}{\partial r}+n(r,t)\frac{\mathrm{d}v(r)}{\mathrm{d}r}\right)\Big|_{r=\sigma} = 0 \tag{7}$$

On the contrary, at the outer boundary the pair density distribution is unaffected, that is,

$$n(r\rightarrow\infty,t) = 1 \tag{8}$$

irrespective of the peculiarities of $w(r)$, the long-time asymptote of Equation (2) obeys the Smoluchowski law, which is characteristic for an infinitely fast contact reaction, however, with an effective reaction radius R_q substituted for the contact distance σ:[28]

$$k(t) = 4\pi R_q D\left(1+\frac{R_q}{\sqrt{\pi D t}}\right) \tag{9}$$

In fact, the asymptotic (Markovian) stationary rate constants $k_\infty = \lim_{t\rightarrow\infty} k(t) = 4\pi R_q D$ extracted from the single photon counting curves for different quencher concentrations and viscosities on the basis of Equations (1) and (9) can be compared with the stationary rates calculated assuming a particular model for the electron transfer rate $w(r)$, that is,[4,23]

$$k_\infty = 4\pi\int_\sigma^\infty r^2 w(r)n_s(r)\mathrm{d}r \tag{10}$$

with $n_s(r)$ denoting the stationary solution of Equation (3) for which $\dot{n}_s=0$. The relative fluorescence intensity, I/I_0, determined in steady state experiments is related to the quencher concentration by the generalized SV law,[4,23]

$$\frac{I}{I_0} = \frac{\int_0^\infty N(c,t)\mathrm{d}t}{\int_0^\infty N(0,t)\mathrm{d}t} = \frac{1}{\tau}\int_0^\infty \exp\left(-\frac{t}{\tau}-c\int_0^t k(t')\mathrm{d}t'\right)\mathrm{d}t$$

$$= \frac{\tilde{R}(0)}{\tau} = (1+c\kappa(c)\tau)^{-1} \tag{11}$$

where $\tilde{R}(s)$ denotes the Laplace transform of $R(t)$. Only in the case of small concentrations the SV rate, κ, will be independent of the quencher concentration c and related to the Laplace transform of $k(t)$, $\tilde{k}(s)$, by:[4,23]

$$\lim_{c\rightarrow 0}\kappa(c) = \kappa_0 = \frac{1}{\tau}\tilde{k}\left(\frac{1}{\tau}\right) \tag{12}$$

The electron transfer rate: For the sink term, $w(r)$, several models have been proposed and evaluated. Among the most popular are the Collins-Kimball model,[15] which assumes a sink at contact, and the exponential model, which in a phenomenological way accounts for the remoteness of the electron transfer step. The latter is exact for Dexter exchange[29] and, since it allows for an analytic solution of R_q as a function of D, it has also gained popularity in recent studies on electron transfer.[28] The most comprehensive model for electron transfer is given by the Marcus expression for single channel diabatic electron transfer:[16–21,30–32]

$$w(r) = \frac{V_\sigma^2}{\hbar}\exp\left(-\frac{2(r-\sigma)}{L}\right)\sqrt{\frac{\pi}{\lambda(r)k_B T}}$$

$$\times\exp\left(-\frac{(\Delta G(r)+\lambda(r))^2}{4k_B T\lambda(r)}\right) \tag{13}$$

which is valid in the normal region and for $V_\sigma \ll k_B T/2$.[33,34] The exponential model has been used to approximate the Marcus expression in the normal region by postulating that their rates at contact and their initial slopes be identical.[28] For the parameter set eventually determined within this work, this approximation is reasonable for high mobilities, however, deviates considerably for the samples at higher viscosities. Thus, we prefer the Marcus model over the exponential one. The Marcus rate has a distinctive distance dependence, which stems from the combined radial dependencies of the free energy change, ΔG, the reorganization energy, λ, and the diabatic coupling matrix element, $V = V_\sigma\exp(-(r-\sigma)/L)$. The reorganization energy comprises contributions from internal changes in the structure of the reactants, λ_i, and the distant dependent solvent reorganization energy, λ_o, which accounts for nonequilibrium solvent polarizations necessary to attain the transition state configuration.[16–21] For solutes of equal size, which is a reasonable approximation in our case (see below), it is given by

$$\lambda(r) = \lambda_i+\lambda_o(\sigma)\left(2-\frac{\sigma}{r}\right) \tag{14}$$

with

$$\lambda_o(\sigma) = \frac{e^2}{4\pi\varepsilon_0\sigma}\left(\frac{1}{n_D^2}-\frac{1}{\varepsilon}\right) \quad (15)$$

The geometry changes upon electron transfer in the present system are small and hence λ_i can be considered negligible compared with λ_o. The latter on the other hand remains virtually unchanged for all the solvent mixtures applied. The radial dependence of the driving force for electron transfer is due to the Coulomb interaction in the products and therefore depends on the static dielectric constant of the medium, ε. The Weller equation[35] yields:

$$\Delta G(r) = E^{ox}(F) - E^{red}(A) - E_{00} - kT\frac{r_c}{r} \quad (16)$$

where r_c denotes the absolute value of the Onsager radius, E_{00} is the energy of the 0–0 transition estimated from the fluorescence and absorption maxima of the fluorophore and $E^{ox}(F)$ and $E^{red}(A)$ are the donor and acceptor oxidation and reduction potentials, respectively. Figure 1 depicts the energy diagram of the electron transfer process relevant to this work.

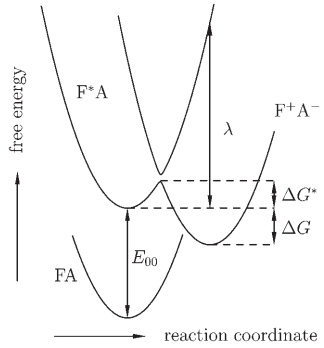

Figure 1. Schematic free energy Scheme for the photoinduced electron transfer (PET) reaction between excited state fluorophore, F*, and quencher, A. The observed reaction proceeds, after photoexcitation of F, from F*A to F^+A^-, overcoming the free energy of activation, ΔG^*. The driving force of the PET, ΔG, is estimated using the 0–0 transition energy of the fluorophore and the reactants ground state redox potentials.

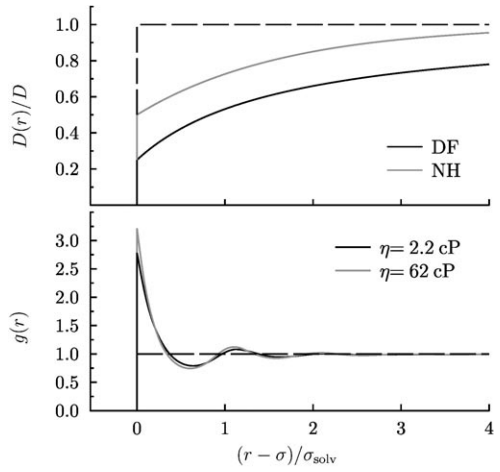

Figure 2. Upper panel shows the spatial dependence of the diffusion coefficient, $D(r)$, using the Deutch and Felderhof (DF), and the Northrup and Hynes (NH) expressions. The lower panel depicts the solvent structures, $g(r)$, obtained from Monte Carlo simulations, for the highest and lowest viscosity solvent mixtures.

Monte Carlo simulations: To obtain the solvent radial distribution function, $g(r)$, we have carried out Monte Carlo simulations at constant volume, number of particles and temperature (MC-NVT simulations).[36–38] The simulations have been conducted on a system of $N_p = 2000$ particles in a cubic box with the particles considered as hard spheres. The simulation box has been chosen cubic for all cases, with a size according to obtain the desired reduced density:

$$\rho^* = \rho\sigma_s^3 \quad (17)$$

where σ_s is the solvent contact radius. A typical simulation consisted of 10^5 Monte Carlo (MC) cycles to equilibrate the system followed by another 10^5 MC cycles to obtain averages. Each MC cycle consisted of N_p attempted displacements of randomly chosen particles. The maximum displacement was adjusted to obtain an averaged acceptance of approximately 40%. Radial distribution functions have been calculated according to:[36,38]

$$g(r^*) = \frac{1}{4\pi N_p\rho^* r^{*2}}\left\langle \sum_i \sum_{i\neq j} \delta(r^*-r_{ij}^*)\right\rangle \quad (18)$$

where $r^* = r/\sigma_s$. In the simulation the Dirac delta function is replaced by unity in a small range of width $l/(2n_{hist})$ around r^*, with l being the size of the simulation box and n_{hist} being the number of divisions used in the histogram set to 200. $g(r)$ was evaluated and accumulated in an histogram with n_{hist} divisions during the simulation.

Numerical procedure: Equation (3), including solvent structure and hydrodynamic hindrance, with the boundary and initial conditions as introduced above, can only be solved numerically. For this purpose the diffusion operator was discretized on a nonuniform grid using well-known finite difference techniques.[39] The grid was adapted to the characteristic decay length of the underlying physical problems, the smallest space increment at contact being 0.01 Å. The inner boundary condition was implemented following Schulten's approach[40] and ensured that the particle conservation requirement was fulfilled. At $r_{max} = 1000$ Å the grid was eventually truncated using the Dirichlet boundary condition $n(r_{max},t) = 1$. The time integration was carried out following the popular, unconditionally stable Crank-Nicolson scheme with nonequidistant time steps and an initial increment of 4 ps. At every discrete time point the cumulative rate constant was calculated using a generalization of Tachiya's approach:[41]

$$\int_0^t k(t')dt' = 4\pi\int (g(r)-n(r,t))dr \quad (19)$$

which follows from Equation (3) and the fact, that the diffusion stencil does not change the number of particles. The reactive pair distribution function thus obtained was utilized to obtain the SV rate, $\kappa(c)$, through Equation (11). The quenching radii, R_q, were evaluated from the stationary pair distribution function, the latter being the solution of the linear system (3) with $\dot{n} = 0$. Unlike for the time-dependent problem, the outer boundary condition was constructed from the asymptotic solution, $n_{asymp} = 1-C/r$, with C being a constant.

Results and Discussion

Frequently, the electron transfer parameters of diffusion influenced quenching reactions are extracted from the non-exponential decay of the time-resolved fluorescence.[22,42] In principle it should be possible to obtain the whole set of parameters from a comprehensive analysis of these decay kinetics, provided that the short time behaviour is fully resolved. In addition no solvent dynamic shifts or similar effects must obscure the quenching decay kinetics. In the present system, using an LED as exciting light source, the latter

requirements are obviously not fulfilled.[43] Nevertheless, the long-time Smoluchowski asymptotics contain relevant information, which can be used to discern between different sets of parameters. In principle R_q, the effective quenching radius, and the diffusion coefficient, D, can be obtained by fitting the convolution of Equation (9) with the instrument response function to the experimental time traces, although it turned out that these two parameters are strongly correlated. In fact, a huge number of D–R_q pairs fit the data equally well. This effect is particularly pronounced at low viscosities, where the transient feature disappears too fast, giving rise to approximately exponential decay curves. An exemplary time trace with the corresponding fit based on Equation (9) is shown in Figure 3. Both the concentration of

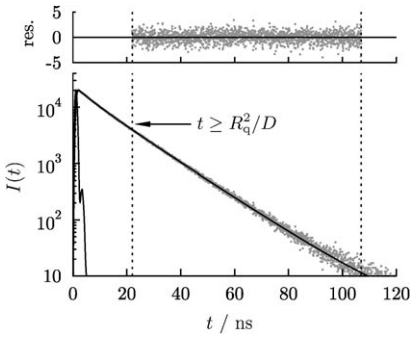

Figure 3. Fluorescence time trace at a quencher concentration of 0.138 M and viscosity of 62 cP. For the indicated range the strongly nonexponential decay is fitted using Equations (1) and (9). In the upper panel the weighted residuals res. $= (I_{exp}-I_{fit})/\sqrt{I_{fit}}$ are given.

the quencher and the viscosity increase the extent of the non-exponentiality of the fluorescence decays (transient effect). It is clear that the observation of this phenomenon is related to the overall efficiency of the quenching process, which depends on the number of quencher molecules in solution and on the duration of the diffusional encounters, R_q^2/D.[23] Thus the non-stationary stage is the longer the higher the viscosity, and the larger in amplitude, the larger the concentration of quencher. The fits to the experimental decays have been performed for times for which Equation (9) holds, that is, $t \geq R_q^2/D$.

Indeed, for the low viscosity samples diffusion coefficients calculated on the basis of the Stokes–Einstein law[44,45] using the stick and the slip boundary conditions, which represent a lower and upper limit for the experimental Ds, invariant values of $k_\infty = 4\pi R_q D$ can be obtained without significantly impairing the quality of the fits. On the other hand at high viscosities the non-stationary feature is sufficiently pronounced to reduce the uncertainty of the values given in Table 1 to $\pm 10\%$. Note that, on principle, k_∞ does not depend on the concentration regardless of the specific diffusion or reactivity model.[7,23] Any deviation from this paradigm would reveal that the actual concentration, c, in the solution deviates from the formal one, as could be due to quencher dimerization, activity coefficient changes or quencher-quencher excluded volume effects. Additionally, an unexpected change in the solvent structure, $g(r)$, with the quencher concentration might give rise to deviations in k_∞. In fact we detect a slight, apparently linear, reduction of k_∞ with concentration, with a slope independent of viscosity. However, this effect does not exceed 15% even at the highest concentrations (0.5 M). Possible effects of the causes mentioned above shall shortly be discussed: Concerning a possible dimerization of the quencher, no dimer formation is apparent from the absorption spectra as mentioned in the Experimental Section. In addition, assuming the same or an increased reactivity of the dimer a parabolic dependence of k_∞ on the quencher concentration ensues, which, however, is not observed experimentally. Only in the limit of totally unreactive dimers an approximate linear dependence of k_∞ on c is obtained which is capable of describing the experimental data with an equilibrium constant of $K = 0.22\,\mathrm{M}^{-1}$. However, given that the quenching radius increases as the dimers form while no significant change in the intrinsic electron transfer parameters ($-k_B RT \ln K = +0.04\,eV!$) occurs, an increased reactivity is to be expected. We thus do not draw on this model in the subsequent analysis. The acceptor–acceptor excluded volume effect on the other hand gives rise to an increase of the effective quencher concentration, which would lead to an increase of the k_∞ with formal concentration, the opposite of what is observed experimentally. The conducted MC simulations predict a small concentration dependence of the solvent distribution function $g(r)$, which, as well, results in a trend opposite to that observed, since the addition of the quencher reduces the height of the maximum in $g(r)$ at σ, and leads to a broadening of the oscillatory features. Moreover, the simulations of R_q with different $g(r)$ values corresponding to different concentrations are apparently undistinguishable. The values of k_∞ reported below are obtained from the linear extrapolation for $c = 0$.

Table 1. Bulk properties of the glycerol/DMSO solvent mixtures and photophysical properties of the fluorophore at 20 °C.[a]

No.	x_{gly}	ρ [g mL^{-1}]	η [cP]	n_D	ε	τ [ns]	$\tilde{\nu}_f$ [kK]	$\tilde{\nu}_a$ [kK]	k_∞ [Å^3 ns^{-1}]
1	0.000	1.10	2.20	1.479	47	22.4	19.0	25.1	3640
2	0.073	1.11	3.31	1.480	49	22.3	19.0	25.1	2760
3	0.150	1.13	5.18	1.480	50	22.4	18.9	25.1	2100
4	0.225	1.14	8.04	1.481	51	22.4	19.0	25.1	1420
5	0.284	1.15	11.67	1.480	51	22.6	18.9	25.1	1080
6	0.351	1.16	17.97	1.479	51	22.6	18.9	25.1	729
7	0.438	1.17	31.93	1.480	51	22.7	18.9	25.0	437
8	0.533	1.19	62.12	1.480	50	22.9	18.9	25.0	257

[a] x_{gly} denotes the mole fraction of glycerol, ρ and η are the mass density and the dynamic viscosity, respectively. n_D and ε denote the refractive index and dielectric constant of the solvent mixture, while τ, $\tilde{\nu}_f$ and $\tilde{\nu}_a$ are the fluorescence lifetime, fluorescence maximum and absorption maximum. k_∞ denotes the stationary quenching rate constant, obtained from the time-resolved measurements.

The SV plots supply an additional set of experimental data that can be used to assign the reaction parameters unambiguously. Representative SV plots are shown in Figure 4. The curvatures and thus the deviations from linearity increase with viscosity due to the increased relative importance of static and non-stationary quenching. Moreover, although apparently linear at first sight, even at the lowest viscosities and most dilute solutions deviations from linearity are observed. Thus, the static and dynamic non-stationary stages are dominating at all concentrations and viscosities.

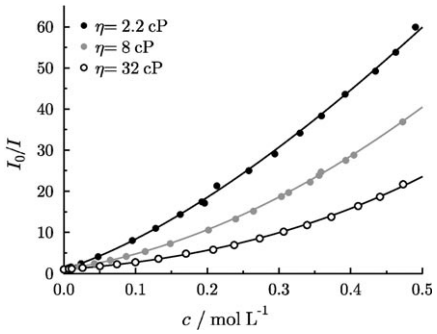

Figure 4. Three representative Stern–Volmer plots showing the strong deviations from linearity at high quencher concentrations.

Six different models, which optionally include the solvent structure and the hydrodynamic effect as summarized in Table 2, have been applied to analyze the data. Models d), e), and f) explicitly account for the solvent structure, with e) and f) additionally including the hydrodynamic effect according to Equations (5) and (6), respectively. Models b) and c) account for the hydrodynamic effect only. It turned out that irrespective of the model used the diffusion coefficients have to be adjusted individually. In particular, none of the common models for diffusion coefficients, that is, the Stokes–Einstein model using the stick or the slip boundary condition or the Spernol–Wirtz model,[46] yielded satisfactory simulation of the experimental data. Even when allowing for an arbitrary, however common, scaling factor we were unable to rationalize the data with a single set of electron transfer parameters (V_σ and L). Thus, the diffusion coefficients were allowed to vary individually during the fitting procedure. This approach led to an excellent reproduction of the experimental SV data irrespective of whether the hydrodynamic effect or the solvent structure had been accounted for (see above). Therefore, solely on the basis of the SV plots it is impossible to decide whether these effects are relevant or not. Table 2 summarizes the results for the six different models. Note furthermore, that any attempts to fit the data with the Collins–Kimball contact approximation severely failed and the assumption of the remote electron transfer step is mandatory. The usage of an hybrid consisting of the Collins–Kimball contact model accounting for non-stationary effects and the sphere of action model accounting for remote static quenching seems paradoxical and was not considered, though it could yield reasonable fits. For all fits the contact distance, σ, has been taken as the sum of the elliptical radii,[47] that is, 8.8 Å, and, if applicable, the solvent diameter, σ_s, was approximated by 5.3 Å. Figure 5 gives an anamorphosis of the SV plots, which show $\kappa=(I_0/I-1)(c\tau)^{-1}$ as a function of c for the most comprehensive model, including $g(r)$ and $D_{DF}(r)$. This representation is better suited than the common SV plot, given in Figure 4, to visualize small changes of the quenching constant and its viscosity dependence. The other models give virtually identical plots, however, with quite different parameters.

For all six models the matrix coupling element, V_σ, was found to be slightly smaller than 1 meV, confirming a diabatic electron transfer reaction. Thus, the dynamic solvent effect, which yields an inverse proportionality to the solvent longitudinal relaxation time,[48,49] can be safely excluded. The tunneling length, L, varies around a value of 2 ± 0.5 Å depending on the model (cf. Table 2). These L values are of similar order of magnitude as those found before by other authors for the reactions between perylene and *N,N*-dimethylaniline[50] or rubrene with duroquinone,[22] for example. Concerning the fitted diffusion coefficients (Figure 6) an inverse relationship with the sample viscosity is to be expected. Actually, this is not the case for any of the models. For the most comprehensive models e) and f) the friction coefficient, f, varies from the stick to the Spernol–Wirtz value or from the Spernol–Wirtz to the slip value on increasing the viscosity, respectively. It has to be considered that a minor influence of the quencher concentration on the viscosity has been observed (at most −10% at the highest concentration and viscosity). This effect, not explicitly accounted for, is compensated during the fit by a decrease of the friction coefficients as the viscosity increases. This is more plausible than considering a viscosity dependent friction coefficient. Any attempt to explicitly consider the measured viscosity at each concentration led, however, to no additional improvements in the results.

While the SV plots do not allow for a distinction between the models used, not all of

Table 2. Comparison of the six models used. σ_{eff} is the diffusion rate constant divided by $4\pi D$ according to Equation (20) and V_σ and L are the matrix coupling element and the tunneling length as extracted from the Stern–Volmer plots.[a]

No.	Model	σ_{eff} [Å]	V_σ [meV]	L [Å]	k_0 (SV) [Å^{3}ns^{-1}]	k_0 (tr) [Å^{3}ns^{-1}]	Residual norm [Å]
a	DET	8.8	0.86	2.5	15200	10400	14.6
b	DET with $D_{NH}(r)$	6.7	0.88	2.6	16400	10400	9.9
c	DET with $D_{DF}(r)$	4.8	0.89	2.7	17100	10000	6.2
d	DET with $g(r)$	9.2	0.73	1.8	15400	17300	5.2
e	DET with $D_{NH}(r)$ and $g(r)$	7.1	0.71	2.1	16300	16300	2.1
f	DET with $D_{DF}(r)$ and $g(r)$	5.2	0.70	2.3	16700	16100	0.4

[a] k_0(SV) is the intrinsic rate constant evaluated using V_σ and L from the Stern–Volmer plots using Eq. (21) and k_0(tr) is the ordinate intercept of the linear regression of k_∞^{-1} versus D^{-1} as described in the text. The residual norm quantifies the deviation from experimental and simulated quenching radii in Figure 7.

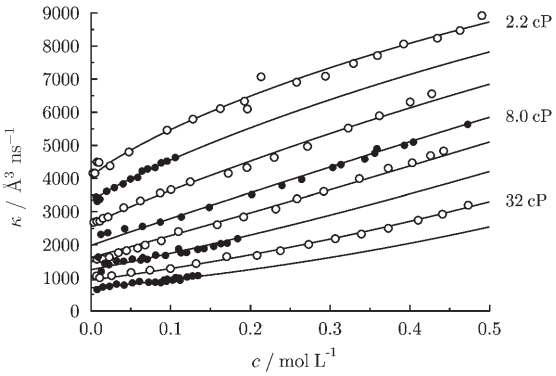

Figure 5. Anamorphosis of the conventional Stern-Volmer plots, allowing for a better appreciation of the simultaneous dependence of κ on concentration and viscosity. Viscosity increases from high to low κ values. All 150 experimental data points are shown. Fits were obtained on the basis of model (f) with the parameters given in Table 2. Fits with the alternative models a)–e) yield virtually indistinguishable fits. However the extracted parameters do not yield satisfactory agreement with the time-resolved experimental evidence (cf. Figure 7).

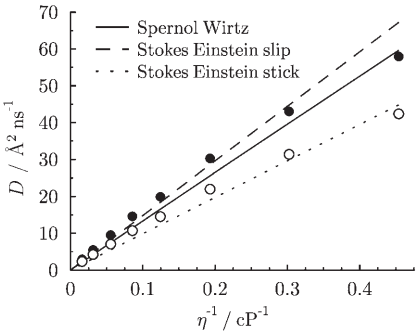

Figure 6. Comparison of the dependence of the diffusion coefficients, obtained from the fits of models (e), open circles, and (f), full circles, to the Stern–Volmer data, with inverse viscosity ($1/\eta$) to those predicted from three diffusion coefficient models (Stokes–Einstein slip and stick, Spernol Wirtz).

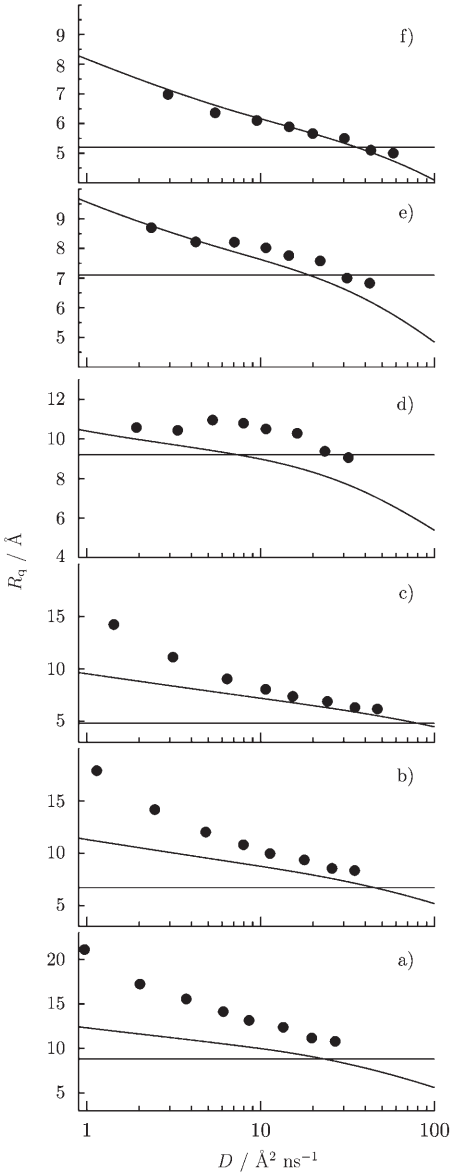

Figure 7. Comparison of the R_q vs D dependence for all models tested. The solid lines give the simulations due to Equation (10) using the parameters extracted from the steady-state data, while bullets refer to the experimental R_q values obtained fits to the long time asymptotic fluorescence decays as described in the text. Only when including the solvent structure, as well as the hydrodynamic effect e)–f) good agreement is achieved. The horizontal lines indicate the quenching radius for a purely diffusion controlled contact reaction for a given model, that is, Equation (20).

them are capable of reproducing the time-resolved data with the ET parameters and diffusion coefficients obtained from the SV fit. For the comparison between steady-state and time-resolved data the R_q versus D plots are compared, where R_q is calculated from $k_\infty/4\pi D$, with k_∞ given by Equation (10) and the D values taken from the fit of the SV plots. Figure 7 gives the R_q versus D plots for all models investigated. In addition, the residual norms obtained from the differences of the experimental and calculated R_q values are summarized in Table 2. The value can be regarded as a quantitative criterion for the ability of the models to concurrently fit the time-resolved and the steady-state experiments. Taking into account both the solvent structure and the hydrodynamic effect reproduce the quenching radii significantly better. Moreover, the R_q/D pairs so obtained fit the fluorescence decays using Equation (9) well, while the simpler models fail. In particular the model of Deutch and Felderhof (see Figure 2) is most suited to reconcile time-resolved and steady-state data. The R_q values can be compared with the effective quenching radii determined for a diffusion controlled contact reaction under the same model conditions. In fact they can be calculated from the following Equation

$$\frac{1}{\sigma_{\text{eff}}} = D \int_{\sigma}^{\infty} D(r)^{-1} r^{-2} \exp(v(r)) \mathrm{d}r \qquad (20)$$

which is easily derived from the steady state solution of the

pair correlation function assuming the Smoluchowski boundary condition, that is, $n(\sigma)=0$. The values for σ_{eff} calculated with Equation (20) are invariant with respect to the viscosity for the first two models, but change by about 1% for the other two due to the composition dependence of the solvent structure. In fact, for a constant D in the absence of any potentials, σ_{eff} certainly equals σ. Obviously, the effective quenching radii for models b), c), e) and f) are smaller than the contact radius obtained from the sum of the vdW radii of the reaction partners. Due to the effectively attractive potential exerted by the solvent structure, σ_{eff} is, however, larger for the most comprehensive models e) and f) as compared to those models where only the reduction of the diffusion rate due to the hydrodynamic hindrance was accounted for.

An additional goodness criterion stems from the comparison of experimentally determined k_0, the kinetic rate of the elementary electron transfer process, and its calculated equivalent. The latter can be obtained from the electron transfer model $w(r)$, which depends on V_σ and L, and the pair correlation function at time zero:[4]

$$k_0 = 4\pi \int_{\sigma}^{\infty} r^2 w(r) n(r,t=0) \mathrm{d}r \qquad (21)$$

Note that for the models including the solvent structure $n(r,0) = g(r)$, whereas it equals unity for the others. The experimental estimates of k_0 can be obtained from the extrapolation of the stationary rate constants, k_∞, to infinitely fast diffusion, that is, from the linear regression of k_∞^{-1} versus D^{-1}. Indeed, for the best model, f), a good linear correlation is found for the experimental points at low viscosities, giving rise to an experimental k_0(tr) of 1.61 10^4 Å^{3}ns^{-1}, which is in very good agreement with the one predicted on the basis of V_σ and L obtained from the steady-state data. An equally good agreement was found for model e), which uses the Northrup Hynes diffusion ansatz. On the contrary no good coincidence between time-resolved and steady-state k_0 values was obtained for the remaining models. It has to be noted, that also the experimental k_0 values depend on the model used, since the experimental k_∞^{-1} are plotted against the diffusion coefficients extracted from the fits to the SV plots.

More insight into the remoteness of the electron transfer encounter can be obtained from the distribution of charged products, $m_0(r)$,[4,23] which is given by

$$m_0(r) = w(r) \int_0^{\infty} n(r,t) N(t) \mathrm{d}t \qquad (22)$$

$4\pi r^2 c m_0(r)\mathrm{d}r$ gives the probability that the electron transfer occurs within the interval r and $r+\mathrm{d}r$ within the time span from 0 to infinity.[51] Figure 8 shows the distance dependence of the normalized initial charge distribution $f_0(r)$ given by:

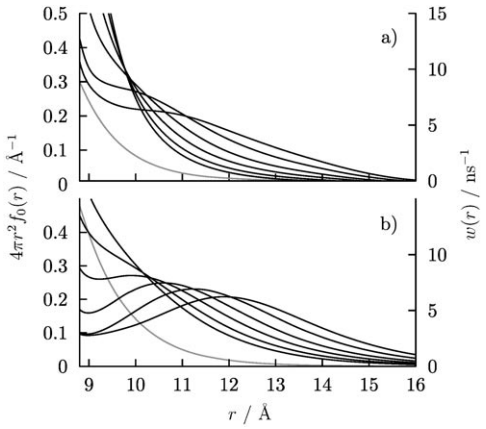

Figure 8. Normalized distribution of charged products for the model including the Deutch–Felderhof treatment of the hydrodynamic effect and the solvent structure (a), and the model including only the former (b), using $c=0.05$ M. The diffusion coefficients are 60, 30, 15, 7.5, 3 and 1 Å^{2}ns with the low values corresponding to the more remote electron transfer. The axis labels on the right refer to the electron transfer rate, $w(r)$ (grey line), calculated using the parameters from table 2.

$$f_0(r) = \frac{m_0(r)}{4\pi \int m_0(r) r^2 \mathrm{d}r} \qquad (23)$$

The distance dependence for two of the models, one including solvent structure and hydrodynamic effect f) and the other including the hydrodynamic effect only c) is shown. A prominent shift of the distribution towards larger r with decreasing D is observed for the model lacking the solvent structure. Thus, as diffusion is slowed down a significant fraction of the quencher molecules react before diffusively reaching the contact surface. On the other hand inclusion of the solvent structure leads to an enhanced static quenching in the near contact region, where the effective potential, $u(r)$, is attractive. Although no maximum ensues, a shoulder in $4\pi r^2 f_0(r)$ at larger r is still observed for small D. For the lowest diffusivity considered the reaction proceeds over a region of approximately 3–4 Å with a nearly constant probability. Thus the inclusion of the solvent structure leads to an enhanced static quenching combined with less pronounced remoteness of the electron transfer.

To put everything into a nutshell, only the most comprehensive models, which explicitly include the solvent structure and the hydrodynamic effect, are able to reproduce well both sets of experimental data, that is, time-resolved and steady-state measurements, with a common set of parameters. This conclusion can, however, only be drawn on the basis of a huge number, in fact 150, experimental points, at eight different viscosities.

Experiments and Procedures

Chemicals and sample preparation: Mixtures of glycerol (Fluka 99.8%, $H_2O \leq 0.01\%$) and dimethylsulfoxide, DMSO (Roth, 99.5%, $H_2O \leq 200$ pp) were applied as solvents, the chemicals being used as received. These

mixtures permit to cover a wide range of viscosities while keeping the solvent and solute properties, among them those governing the electron transfer, that is, dielectric constant, ε, and refractive index, n_D, constant (cf. Table 1). This has been experimentally verified for the used solvent mixture in ref. [52]. In particular the Pekar factor, $\gamma = n_D^{-2} - \varepsilon^{-1}$, remains virtually unchanged, with an average value given by 0.46.[53]

The fluorophore 2,5-bis(dimethylamino)-1,3-benzenedicarbonitrile, *F*, was synthesized and purified as described in ref. [54] ($E^{ox}(F) = 0.73$ V vs SCE). The quencher, 1,3-dimethyl-2-nitrobenzene, *A*, (Aldrich, 99%) was distilled under reduced pressure ($E^{red}(A) = -1.40$ V vs SCE[55]). A liquid quencher was chosen to avoid solubility problems at high concentrations of quencher at high viscosities. Additionally *A* holds the advantage of having a similar refractive index ($n_D(A) = 1.522$) as the solvent mixtures used, thus not altering the solutions' refractive index even at highest concentrations added. At the same time the fluorophore exhibits a virtually unchanged quantum yield ($\Phi_f \approx 0.55$) and a long fluorescence lifetime, τ, which allows for an extraction of the stationary quenching rate constant, k_∞, from the fluorescence decay asymptotics within the limits of the used model. Additionally *F* has a vanishing intersystem crossing quantum yield, relatively simple photophysics,[43] undergoes reversible electrochemical $1-e^-$ oxidation and shows no ground state complex formation with *A* (cf. Figure 9). Summarizing the system allows for varying the viscosity only, while keeping the rest of the intrinsic solvent properties constant.

Both solvent mixtures and sample solutions were prepared by weighing

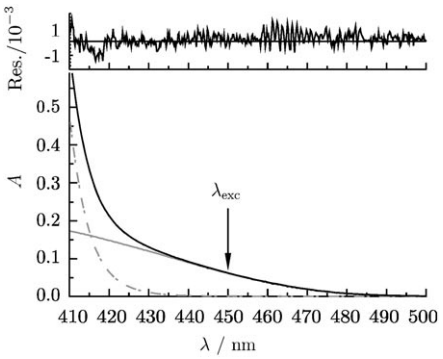

Figure 9. Decomposition of the sample absorption spectrum (black line) into individual fluorophore (grey full line) and quencher (grey dash-dotted line) absorption spectra. The excitation wavelength is indicated by an arrow.

in the individual components. The lowest viscosity samples (2.2 and 3.3 cP) were deaerated (bubbling with argon for 15 minutes; absorption spectra taken after deaeration) to avoid interference by fluorescence quenching due to dissolved oxygen, which was not necessary for higher viscosities. The hygroscopicity of DMSO and glycerol made it necessary to perform the measurements in septa-sealed quartz cuvettes (10 mm Suprasil glass). The concentration of *F* was always set such that the absorption at the excitation wavelength (430 to 445 nm) did not exceed 0.10, corresponding to a maximum concentration of 10^{-4} M. All experiments were performed at 20 ± 0.2 °C.

The two solute molecular radii ($r_F = 4.8$, $r_A = 4.0$ Å) were obtained by circumscribing the geometry optimized van der Waals surfaces with ellipsoids of minimal surface. The solvent diameters ($\sigma_{gly} = 5.47$, $\sigma_{dmso} = 5.13$ Å) were taken from the literature.[56]

Apparatus: Absorption spectra were recorded with a Shimadzu UV-3101PC UV-VIS-NIR spectrophotometer using a bandpass of 1 nm. The true fluorophore and quencher concentrations were obtained by separating the sample absorption spectra into the arithmetic sum of the individual quencher and fluorophore absorption spectra. Steady-state fluorescence spectra were obtained by connecting an isolated temperature controlled aluminium block (sample compartment) via light guides to a Jobin-Yvon Spex FuoroMax-2 spectrofluorimeter (scan range from 250 to 900 nm). The fluorescence intensities, used for the SV plots, were taken as the integrals of the obtained fluorescence spectra (starting the integration 10 nm above the excitation wavelength) and corrected for the true fluorophore concentration and inner filter effect. For the latter a similar correction as in[57] was applied, but taking the limits of an infinitely thin emitting light beam ($\Delta X = 0$) coming from the centre of the cuvette ($X = 0.5$). The overall correction applied to the observed light intensity, I_{obs}, is as follows:

$$I_{corr} = \frac{I_{obs}}{c_F} 10^{A/2} \text{ with } A = \int f(\lambda) \mathrm{OD}(\lambda) \mathrm{d}\lambda \quad (24)$$

where *A* is the sample absorption at the excitation wavelength (taking into account the fluorescence spectrometer bandpass, given by $f(\lambda)$), OD denotes the optical density of the sample, and c_F denotes the relative fluorophore concentration with respect to I_0, the intensity when no quencher is present.

Time-resolved measurements (TCSPC method, for a thorough description of the used apparatus consult[58]) were performed in the same block as the steady-state experiments exciting with unpolarized light from a 450 nm LED (PicoQuant, FWHM ≈ 1 ns). In the emission beam a 550 nm longpass filter was used to avoid interference with scattered excitation light. Both, steady-state and time-resolved experiments, were performed without using polarisers. Firstly, because in the time-resolved experiments the usage of a 550 nm longpass filter in the time resolved setup led to the observation of a dynamic solvent shift, which manifests itself in an initial increase of the fluorescence time traces (at the highest viscosity with $\tau \approx 1$ ns) superimposed on any small, though possibly present, anisotropy effects. Secondly, due to the long fluorescence lifetime, the moderate quenching (especially at high viscosities), the very short rotational correlation times (as estimated from the fluorescence decays without quencher), and the usage of totally unpolarized excitation light, the impact of polarisation effects on the steady-state data was, unlike in ref. [12], found to be negligibly small ($\ll 1\%$).

Dynamic viscosities, η, were obtained using $\eta = \nu\rho$ where ν is the kinematic viscosity, which was measured by means of a thermostatized capillary Ubbelohde viscosimeter (Schott) and ρ is the density which was measured using a pycnometer. The refractive indices, n_D, were determined using a temperature controllable Abbé refractometer (1T model from Atago). The solvent mixtures' dielectric constants, ε, were taken from ref. [52]. Mixture compositions and properties are summarized in Table 1.

Conclusions

In an extensive study comprising 150 data points, recorded at eight different viscosities and spanning a large concentration range, we have shown that the electron transfer quenching of fluorescence can be modelled by DET. Taking into account the solvent structure and the hydrodynamic effect it is possible to coherently explain both the time-resolved and the steady-state experiments assuming a remote electron transfer reaction. No consistent description of all the data is possible without including these features simultaneously. This conclusion can only be achieved thanks to the big number of quencher concentrations studied in the bending region of the SV plots. While either a separate analysis of the time-resolved and the steady-state data or a lower number of experimental points, can yield satisfactory fits, time-resolved and steady-state results can only be reconciled in a comprehensive and exhaustive study as the one presented here. Otherwise, the extracted electron transfer parame-

ters may be biased or not based on physical grounds. Furthermore, a critical study on the diffusion models would not be possible. In summary, we have shown that only by correctly accounting for diffusion, including the hydrodynamic effect and the solvent structure, a comprehensive description of fluorescence quenching by photoinduced electron transfer at moderate to high viscosities is possible.

Acknowledgements

D.K. and A.R. would like to thank Nikita Lukzen, Alexandra Yurkovskaya and Konstantin Ivanov for helpful discussions during their stay at the International Tomography Center, Novosibirsk. G.G. thanks Masanori Tachiya for the hint on using Equation (19) for the time integration. A.C. thanks Nederlandse Organisatie voor Wetenschappelijk Onderzoek (NWO) for financial support. The authors are thankful to Patrice Jacques for stimulating discussions concerning the manuscript.

[1] J. B. Birks, *Photophysics of Aromatic Molecules*, Wiley Monographs in Chemical Physics, Wiley-Interscience, London, **1970**.
[2] G. J. Kavarnos, *Fundamentals of Photoinduced Electron Transfer*, VCH, New York, **1993**.
[3] B. Valeur, *Molecular Fluorescence: Principles and Applications*, Wiley-VCH, Weinheim, **2001**.
[4] A. I. Burshtein, *Adv. Chem. Phys.* **2000**, *114*, 419–587.
[5] L. Burel, M. Mostafavi, S. Murata, M. Tachiya, *J. Phys. Chem. A* **1999**, *103*, 5882–5888.
[6] J. R. Lakowicz, *Top. Fluoresc. Spectrosc.* Plenum Press, **1991**, Chapter 2.
[7] A. V. Popov, V. S. Gladkikh, A. I. Burshtein, *J. Phys. Chem. A* **2003**, *107*, 8177–8183.
[8] R. Cukier, *J. Am. Chem. Soc.* **1985**, *107*, 4115–4117.
[9] S. Vavilov, *Z. Phys.* **1929**, *53*, 665–674.
[10] J. Keizer, *Chem. Rev.* **1987**, *87*, 167–180.
[11] B. Stevens, D. N. McKeithan, *J. Photochem. Photobiol. A* **1989**, *47*, 131–141.
[12] J. C. André, M. Bouchy, W. R. Ware, *Chem. Phys.* **1979**, *37*, 119–131.
[13] S. M. B. Costa, A. I. Macanita, S. J. Formosinho, *J. Phys. Chem.* **1984**, *88*, 4089–4095.
[14] M. von Smoluchowski, *Z. Phys. Chem.* **1917**, *92*, 129–168.
[15] F. C. Collins, G. E. Kimball, *J. Colloid Sci.* **1949**, *4*, 425–437.
[16] R. Marcus, *J. Chem. Phys.* **1956**, *24*, 966–978.
[17] R. A. Marcus, *J. Chem. Phys.* **1956**, *24*, 979–989.
[18] R. A. Marcus, *J. Chem. Phys.* **1957**, *26*, 867–871.
[19] R. A. Marcus, *Discuss. Faraday Soc.* **1960**, *29*, 21–31.
[20] R. A. Marcus, H. Eyring, *Annu. Rev. Phys. Chem.* **1964**, *15*, 155–196.
[21] R. A. Marcus, *J. Chem. Phys.* **1965**, *43*, 679–701.
[22] S. F. Swallen, K. Weidemaier, H. L. Tavernier, M. D. Fayer, *J. Phys. Chem.* **1996**, *100*, 8106–8117.
[23] A. Burshtein, *Adv. Chem. Phys.* **2004**, *129*, 105–418.
[24] N. N. Tunitskii, K. S. Bagdasar′yan, *Opt. Spectrosc.* **1963**, *15*, 100–106.
[25] S. A. Rice, *Diffusion-Limited Reactions, Vol. 25 of Comprehensive Chemical Kinetics*, Elsevier, Amsterdam, **1985**.
[26] S. H. Northrup, J. T. Hynes, *J. Chem. Phys.* **1979**, *71*, 871–883.
[27] J. Deutch, B. U. Felderhof, *J. Chem. Phys.* **1973**, *59*, 1669–1671.
[28] V. S. Gladkikh, A. I. Burshtein, H. L. Tavernier, M. D. Fayer, *J. Phys. Chem. A* **2002**, *106*, 6982–6990.
[29] D. L. Dexter, *J. Chem. Phys.* **1953**, *21*, 836–850.
[30] V. Levich, R. Dogonadze, *Dokl. Akad. Nauk SSSR* **1959**, *124*, 123–126.
[31] V. Levich, R. Dogonadze, *Collect. Czech. Chem. Commun.* **1961**, *26*, 193–214.
[32] V. Levich, *Adv. Electrochem. Eng.* **1966**, *4*, 249–371.
[33] I. Rips, J. Jortner, *Chem. Phys. Lett.* **1987**, *133*, 411–414.
[34] I. Rips, J. Jortner, *J. Chem. Phys.* **1987**, *87*, 2090–2104.
[35] A. Weller, *Z. Physik. Chem. N. F.* **1982**, *130*, 129–138.
[36] D. Frenkel, B. Smit, *Understanding Molecular Simulation*, Academic Press, San Diego, **1996**.
[37] D. P. Landau, K. Binder, *A Guide to Monte Carlo Simulations in Statistical Physics*, Cambridge University Press, **2000**.
[38] M. P. Allen, D. J. Tildesley, *Computer Simulation of Liquids*, Clarendon Press, Oxford University Press, **1987**.
[39] J. Crank, *The Mathematics of Diffusion*, Oxford University Press, 2nd ed., **1980**.
[40] H.-J. Werner, Z. Schulten, K. Schulten, *J. Chem. Phys.* **1977**, *67*, 646–663.
[41] M. Tachiya, *Radiat. Phys. Chem.* **1983**, *21*, 167–175.
[42] S. Murata, S. Matsuzaki, M. Tachiya, *J. Phys. Chem.* **1995**, *99*, 5354–5358.
[43] A. Rosspeintner, G. Angulo, M. Weiglhofer, S. Landgraf, G. Grampp, *J. Photochem. Photobiol. A* **2006**, *183*, 225–235.
[44] A. Einstein, *Ann. Phys.* **1905**, *17*, 549–560.
[45] A. Einstein, *Ann. Phys.* **1906**, *19*, 371–381.
[46] A. Spernol, K. Wirtz, *Naturforsch.* **1953**, *8a*, 522–532.
[47] G. Grampp, W. Jaenicke, *Ber. Bunsenges. Phys. Chem.* **1991**, *95*, 904–927.
[48] L. Zusman, *Chem. Phys.* **1980**, *49*, 295–304.
[49] A. Barzykin, P. Frantsuzov, K. Seki, M. Tachiya, *Adv. Chem. Phys.* **2002**, *123*, 511–616.
[50] G. Angulo, G. Grampp, A. A. Neufeld, A. I. Burshtein, *J. Phys. Chem. A* **2003**, *107*, 6913–6919.
[51] S. Murata, N. Tachiya, *J. Phys. Chem.* **1996**, *100*, 4064–4070.
[52] G. Angulo, PhD thesis, Institute of Physical and Theoretical Chemistry, TU Graz (Austria), **2003**.
[53] B. Bhattacharyya, J. Wolff, *J. Biol. Chem.* **1984**, *259*, 11836–11843.
[54] G. Schwarzenbacher, B. Evers, I. Schneider, A. de Raadt, J. Besenhard, R. Saf, *J. Mater. Chem.* **2002**, *12*, 534–539.
[55] L. Meites, P. Zuman, *CRC Handbook Series in Electrochemistry, Vol. I–V*, CRC Press, Boca Raton, FL, **1977–1982**.
[56] Y. Marcus, *The Properties of Solvents*, Wiley Series in Solution Chemistry, Wiley, **1998**.
[57] I. E. Borissevitch, *J. Lumin.* **1999**, *3*, 219–224.
[58] S. Landgraf, *Spectrochim. Acta Part A* **2001**, *57*, 2029–2048.

Received: January 22, 2007
Published online: May 10, 2007

